

Magnetic coupling and electric conduction in oxide diluted magnetic semiconductors

H. Chou,^{1,*} C. P. Lin,¹ J. C. A. Huang,² and H. S. Hsu^{1,2}

¹*Department of Physics and Center for Nanoscience and Nanotechnology, National Sun Yat-Sen University, Kaohsiung, Taiwan 804, Republic of China*

²*Department of Physics, National Cheng Kung University, Tainan, Taiwan 701, Taiwan*

(Received 19 January 2008; published 25 June 2008)

The mechanism for the room temperature magnetic coupling and electric conduction in oxide diluted magnetic semiconductors (DMSs) has been simultaneously studied on the Co:ZnO thin film by utilization of the electric field effect. We find that the carriers are bound on a defect in a radius much larger than the bounded magnetic polaron (BMP) radius and can move by variable-range hopping (VRH) over a relatively small distance. Here, we propose a concentric bounded model consisting of a concentric localization configuration with a limited carrier VRH capability. In this model, the carriers localized around defects strongly couple with the doped magnetic ions forming a BMP in the inner sphere and can only itinerate with no spin coherence in the outer shell. Carriers can hop either by spin-polarized or by spin-independent VRH directly between or not directly between adjacent inner spheres, respectively. This model can explain both the electric and magnetic properties of the oxide DMS and depicts an evolution of electric and magnetic properties associated with defect concentration. The spin-current ratio depends on the ratio of the inner and outer radii.

DOI: [10.1103/PhysRevB.77.245210](https://doi.org/10.1103/PhysRevB.77.245210)

PACS number(s): 72.25.Dc, 72.20.Ee, 75.30.Hx, 75.50.Pp

I. INTRODUCTION

Since the discovery of diluted magnetic semiconductors (DMSs),^{1–4} extensive study on the mechanism and its application in science and in devices has proven DMS a potential material for realization of spintronics.⁵ Although III-V and II-VI DMS were discovered to have the greatest possibility in integrating with the present semiconducting technique, its low ferromagnetic (FM) transition temperature—below room temperature—limits further application. As Dietl *et al.*^{6,7} pointed out, room temperature DMS may occur in a large band gap material such as GaN and ZnO by doping suitable magnetic ions. Among these, because ZnO is one of the candidates for the next generation transparent semiconductor, transition metal doped^{8–10} or nitrogen substituted ZnO (Ref. 11) has attracted great attention for its magnetic properties. However, the introduced magnetic ions are so diluted that a direct magnetic exchange is less likely, and oxide DMS usually exhibits a low conductivity so that indirect Ruderman–Kittel–Kasuya–Yosida (RKKY) coupling, which is one of the main coupling mechanisms in III-V and II-VI DMS materials,^{12–14} is incongruent with the experimental data. It was proven that the magnetic coupling in oxide DMS is carrier mediated.^{6,13,15,16} Unlike the RKKY model, in which the mediated carriers are free carriers, the effective carrier in oxide DMS seems to be localized by oxygen vacancies in hydrogen-like orbits. When the carrier concentration exceeds a certain value, an impurity band is formed.^{17–19} Whenever magnetic dopants sit inside the radius of and couple with localized carriers, a bounded magnetic polaron (BMP) is formed. Once the overlapping of BMPs crosses over the entire sample, bulk ferromagnetism is created.^{6,18–25}

This fascinating model provides a possible explanation for the magnetic mechanism of oxide DMS that used to be obscured. However, only a few indirect experiments, such as the high resistivity of samples and the ferromagnetism's dependence on the concentration of defects,^{13,23,26–28} support

this model. Both how the carriers are localized in the BMP model and how they produce their finite conductivity remain unclear. In this study, we employ the electric field effect on and measure the transport properties of the Co:ZnO thin film as an example to understand the mechanism of magnetic coupling and electric conduction for oxide DMS, respectively. By applying electric fields, magnetic characteristics are measured when carriers are injected to or extracted from the film. We find that the deviation of carrier concentration in a limited range does not affect the values of the saturated magnetization and the coercivity, but does, in fact, affect the tendency to reach the saturated magnetization. These magnetic phenomena can quite accurately be explained by the BMP model in that the injection or extraction of carriers corresponds to the shrinking or expanding radius of the hydrogen orbits. However, the localization of the radius of carriers estimated from transport measurements is larger than that of the BMP model by a factor of 3. This strongly implies that the BMP alone is not enough to describe the electric property. By considering the larger localization radius, a concentric bounded model that can explain the magnetic coupling and carrier hopping is proposed.

II. EXPERIMENT

Sample growth was carried out in an ion beam sputter system by multilayer δ -doping technique. The $[\text{Co}(1 \text{ \AA})/\text{ZnO}(n\text{\AA})]_{25}$ ($n \geq 15$) multilayers were deposited on epitaxial grade $\alpha\text{-Al}_2\text{O}_3$ (0001) substrates at room temperature. Magnetic impurities, i.e., Co, were produced by sandwiching a 1 \AA Co layer between two adjacent $n\text{\AA}$ ZnO layers. The superstructure was reproduced 25 times. These samples were proven to be good substitutional (Co^{2+} substituted for Zn^{2+}) structures by performing rigorous structural characterizations, such as x-ray absorption and transmission electron microscopy measurements.^{27,28} Due to the high resistivity of samples at low temperature, the electric resistivity

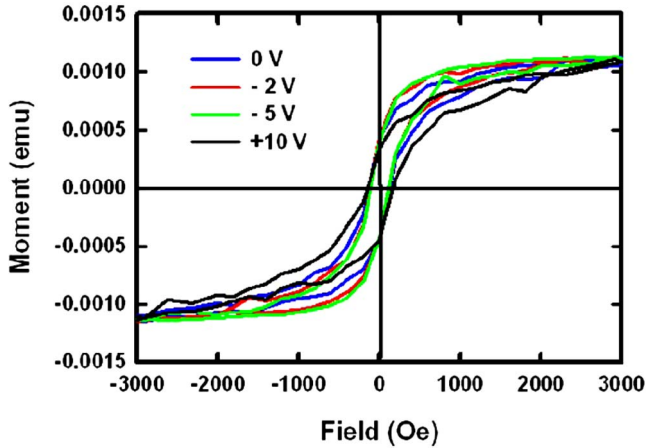


FIG. 1. (Color online) Electric field effect on 1:17 Co:ZnO films. The positive and negative bias voltages represent the injection and extraction of electron carriers to the film. 10 V is equal to an injection of 2×10^{17} carriers per cm^3 , which is approximately one-tenth of the total carrier concentration of the film.

as a function of temperature is measured by four or two point geometry. To apply an electric field, a 2000 Å Au film and 50 Å Al_2O_3 insulator layer were deposited on top of the Co:ZnO film. The final sample was then placed in a superconducting quantum interference device to measure the magnetic hysteresis at room temperature while swiping the electric field.

III. RESULTS AND DISCUSSION

Figure 1 shows several hysteresis curves under various bias electric voltages, V_b . The electric field built up by the external dc source can be as large as 2×10^7 V/cm at $V_b = 10$ V, and the correspondent injected or extracted carrier concentration reaches 2×10^{17} cm^{-3} , which is approximately 2 orders lower of the carrier concentration of our 1:15 films. When V_b is swiped within ± 10 V, the saturated magnetization and the coercivity of the film remain at the same value and do not change with the external voltage. Nevertheless, the trend of a magnetization curve from a remnant to a saturated magnetization changes with different V_b . For $V_b = +10$ V, the magnetization gradually increases in the positive field, reaching a saturated magnetization M_s at around 3000 Oe. When the bias is changed to -5 V, the magnetization saturates much faster at around 1500 Oe.

The BMP model with the specific modification we introduce here can fully explain the magnetic phenomena observed in the present experiment. It is known that the carrier may be contributed from oxygen vacancies,^{23,26} magnetic dopants, Zn interstitials,^{10,13,29} or other kinds of defects. When a film is grown, all those defects are in fixed positions and concentrations. The injection or extraction of carriers by the applied electric field only varies in concentration at the lowest point of a conduction band, which overlaps with the localized impurity band where most carriers are bounded around oxygen vacancies as the BMP model describes.²⁴ Since the magnetic dopants, Co ions, have the same valence

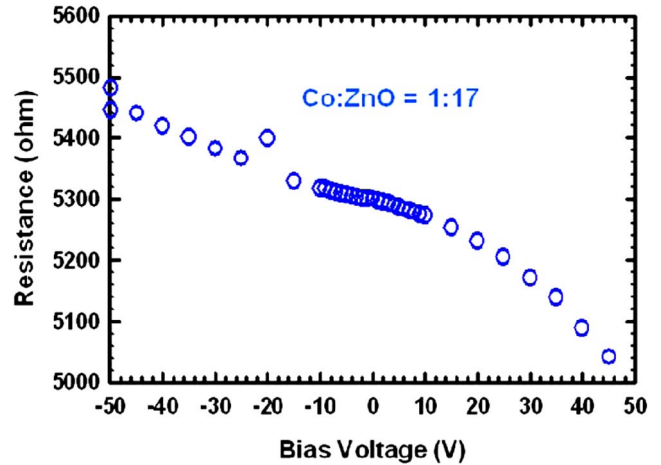


FIG. 2. (Color online) Resistance of the film as a function of electric bias voltages. The resistance of the film increases or decreases with the injection or extraction of carriers, respectively. A linear relationship is observed within ± 10 V of bias.

as Zn ions and can be assumed to have no other noticeable defects besides the oxygen defects in our film, it is reasonable to estimate the defect concentration by measuring the carrier concentration of the normal Hall measurement. The carrier concentration of our film is around the order of 10^{19} cm^{-3} . If all defects are in a uniform distribution and if all BMP are centered on those defects, the BMP spheres are far from the overlapping necessary for FM coupling in the BMP model. If, however, an unknown coupling mechanism, such as an inhomogeneous distribution of defects, provides a magnetic exchange coupling between those close, but not overlapping, BMP spheres, a FM phase should form when a percolation of those couplings throughout the entire sample is created. The increase in the carrier concentration by the electric field injection increases the effective mass of bounded carriers, and vice versa. According to the BMP model, $r_H = \epsilon(m/m^*)a_0$, the increase in the effective mass reduces the bounded radius and, thus, the separation of BMP spheres increases and the magnetic coupling decreases. As a result, a larger applied magnetic field is needed to align moments in order to reach the saturated magnetization. When the applied electric voltage is switched from positive to negative, as in the example of -5 V as plotted by a green curve, the carrier concentration and the distance between BMP spheres decrease, so that the magnetization saturates faster. Because the change in carrier concentration by the electric field is only at around 1% of the total carrier concentration of the film, the change in BMP radius is small. This small change in the bounded radius does not vary the number of magnetic dopants that are included and, therefore, the saturated magnetization and coercivity do not change with the electric field.

The resistance of the film may also be altered by applying an external electric field. Applying a positive electric field injects donor electrons that increase the carrier concentration, while applying a negative field extracts the donor carriers. The resistance while applying bias voltage is plotted in Fig. 2 and follows a nearly linear response to the applied voltage

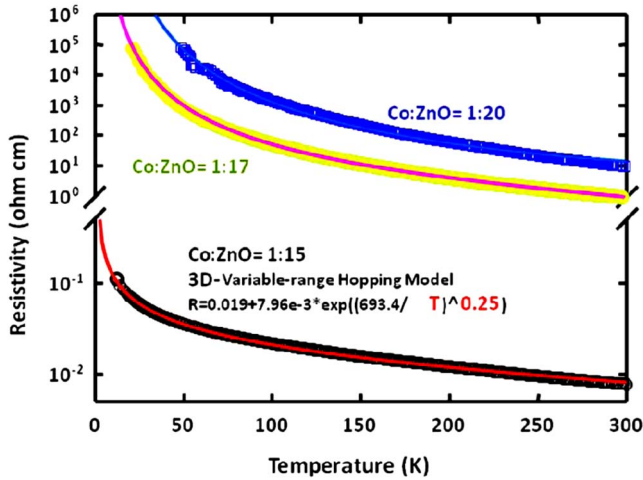


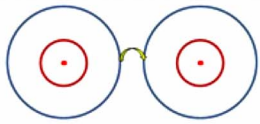
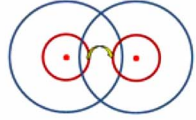
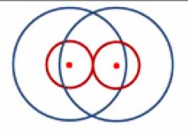
FIG. 3. (Color online) Resistivities of Co:ZnO films (with 1:15, 1:17, and 1:20 ratios) as a function of temperature at zero electric bias voltage. Under the same growth conditions, the resistivity increases with an increase in the thickness of the ZnO layers or with a decrease in the concentration of Co dopants. This strongly suggests that the magnetic dopants initiate the formation of defects that supply the necessary carriers for the electric conduction. All ρ - T curves can be fitted quite well by Mott's VRH model. Films of 1:15 and 1:17 can be fitted by the 3D variable-range hopping model and those of 1:20 can better fit the 2D variable-range hopping model.

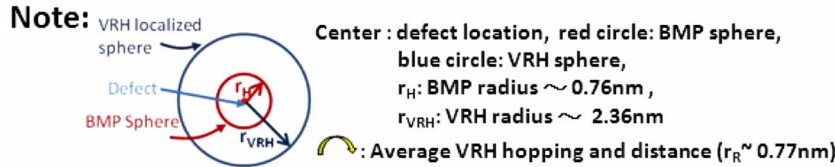
when V_b is within ± 10 V. The resistance decreases while applying a positive bias, and vice versa. This strong association between the injected and extracted carriers with both magnetic and electric properties cannot be described solely by the simplified BMP model. The carrier hopping or coulomb coupling between on site carriers may play some roles. The resistivity as a function of temperature (ρ - T) curves at zero magnetic field are plotted in Fig. 3. These three films were all grown in the same growth conditions except for the thickness of the inserted ZnO layers. The resistivity dramatically increases for films with thicker ZnO layers. The resistivity of a pure ZnO film with the same thickness exhibits an extremely high resistance and can be regarded as a pure insulator. Thicker ZnO layers contain lower concentrations of magnetic dopants. It is clear that the doped magnetic impurities act like a catalyst that initiates the formation of defects around it. These ρ - T curves can be described by Mott's variable-range hopping (VRH) model,³⁰ $\rho = \rho_0 \exp[(T_0/T)^d]$. The films with Co:ZnO ratios of 1:15 and 1:17 exhibit a three-dimensional (3D) ($d=1/4$) VRH, while those of 1:20 can be described by a quasi-two-dimensional ($d=1/3$) VRH. The 1:15 film, the thickness limit of ZnO layers for not forming Co clusters, has a 3D distribution of Co ions and, because the film has a resistivity very similar to that of CMR materials, we use similar parameters³¹ in the VRH model to understand the transport phenomenon. Accordingly, the VRH fitting of the 1:15 film gives two important parameters: the VRH localization radius [$r_{\text{VRH}} = 1/\alpha$ and $k_B T_0 = 18\alpha^3/N(E_F)$, where T_0 and $N(E_F)$ are the exponent parameter of VRH and the density of state at the Fermi level, respectively] and the average VRH distance ($r_R = 3R/4$, with $R = 3^{1/4}/[2\pi\alpha N(E_F)k_B T]^{1/4}$). The former reveals the range of

a carrier localized by a defect in a hydrogenic orbit and the latter reflects the average distance that a carrier can hop out of the VRH sphere. It is found that $r_{\text{VRH}} \sim 2.36$ nm and $r_R \sim 0.77$ nm. The VRH localized length is about a factor of 3 times the oxygen vacancy constituted BMP localized radius ($r_{\text{BMP}} \sim 0.76$ nm for the ZnO material) as reported by Coey. Because the localized centers for BMP and VRH spheres originate in the same kinds of defects, it is highly possible for them to overlap at the same defect sites. This suggests that carriers are localized around a defect with a hydrogenic orbit in a large sphere that has a radius of 2.36 nm; however, the localized carrier can only form a bounded magnetic polaron with magnetic dopants inside the smaller BMP sphere within a radius of 0.76 nm. With these data, the localization model of a carrier around a defect may now be modified as a concentric bounded model, as shown in Table I, with the center as the defect site, and surrounded by a small and a large circle representing the BMP and VRH spheres, respectively. When the localized carrier is itinerating in the shell with a radius r between r_{BMP} and r_{VRH} (i.e., $r_{\text{BMP}} < r < r_{\text{VRH}}$), the carrier may not maintain its spin in coherence. Interestingly, the VRH distance ($r_R \sim 0.77$ nm) is the same as the BMP radius ($r_{\text{BMP}} \sim 0.76$ nm). If, however, the density of states at the Fermi energy in the present sample may be lowered, then in colossal magnetoresistance (CMR) materials, due to the defect initiated shallow donor level, both the VRH localization radius and the VRH distance should become larger than this estimated. The truth that the VRH localization radius is larger than the radius of the BMP model remains.

Table I elaborates the configuration of the concentric bounded model and the possible hopping situations. Figure 4 illustrates the phase and magnetization evolutions associated with the coupling situations in Table I as a function of the defect concentration for the uniform and inhomogeneous distributions. When the defect concentration is extremely low, these concentric spheres are distributed far enough apart such that the localized carrier has no chance to hop from one sphere to another, and is therefore unable to conduct, and the magnetic dopants cannot couple to one another. Therefore, the sample should exhibit a paramagnetic insulator, shown as the "insulator PM" state in Fig. 4. With an increase in defects, such as oxygen defects caused by growing films in vacuum or by postannealing in hydrogen, the concentric circles may approach each other to a separation distance equal to or smaller than the VRH distance r_R , shown as the first case in Table I. In this case, the localized carrier has an opportunity to hop from one sphere to the adjacent one. The sample becomes VRH conducting with a high resistivity. Since a direct hopping of carriers cannot be built within two BMP spheres, the sample remains in a paramagnetic state. For this case, the ideal separation between two defects is about 4.72 nm, which corresponds to 0.0036% of the total oxygen ions or a carrier concentration of 2.9×10^{18} cm⁻³. This carrier concentration is lower than that of our present films, which have FM characteristics. If, however, the distribution of magnetic dopants may be driven by attractive forces between magnetic ions as Kuroda *et al.*³² reported in the Cr:ZnTe sample, a slightly inhomogeneous distribution of spheres due to the possible formation of VRH sphere clus-

TABLE I. (Color online) Illustration of the concentric localization model and the corresponding parameters. Note: center, defect location; red circle, BMP sphere; blue circle, VRH sphere; r_H , BMP radius ~ 0.76 nm; r_{VRH} , VRH radius ~ 2.36 nm; \bar{r}_R average VRH distance ($r_R \sim 0.77$ nm); d_d , the distance between defects; ρ_d , the defect concentration; ρ_o , the oxygen defect percentage (if all defects are oxygen defects); ρ_c , the carrier concentration (if carriers are from oxygen defects only); the number of magnetic dopants in a BMP sphere for the present film = 9.7; and the number of magnetic dopants in a VRH sphere for the present film = 291.8.

	Coupling	type	d_d (nm)	ρ_d ($\times 10^{25}$ cm^{-3})	ρ_o %	ρ_c cm^{-3}
1		VRH Rest \gg PM	5.49	0.144	0.0036	2.9×10^{18}
2		VRH Rest $>$ FM \ll	2.29	1.99	0.05	4×10^{19}
3		VRH Rest $<$ FM $>$	1.52	6.8	0.17	1.4×10^{20}



d_d : the distance between defects
 ρ_d : the defect concentration
 ρ_o : the oxygen defect percentage (if all defects are oxygen defects)
 ρ_c : the carrier concentration (if carriers are from oxygen defects only)
 The number of magnetic dopants in BMP circle for the present film = 9.7
 The number of magnetic dopants in VRH circle for the present film = 291.8

ters or a percolation path may promote the hopping of spin-polarized carriers inside a BMP sphere to another BMP sphere. The clusters that act as magnetic polarons may grow in size with an increase in defects, and therefore, result in superparamagnetism. Further, the percolation of VRH spheres provides an opportunity for spin-polarized and localized carriers to hop through the path, which initiates a very weak bulk ferromagnetism.

When more oxygen vacancies are introduced, the concentric spheres overlap with one another and a direct hopping of a localized carrier between two BMP spheres becomes possible, shown as the second case in Table I. It is reasonable to assume that the hopping is a spin-polarized hopping within two BMP spheres because the average VRH distance is only 0.77 nm. The overlapping of VRH spheres makes the sample VRH conductive and the correlation of two BMP spheres causes the sample to be weakly FM, shown as the “VRH-conduction weak FM” state in Fig. 4. In this case, the distance between two adjacent defects is 2.29 nm, which corresponds to a concentration of carriers of $4 \times 10^{19} \text{ cm}^{-3}$, approximately equal to the carrier concentration of the 1:15

film. With the possible inhomogeneous distribution of defects, a percolation can be initiated at a lower defect or carrier concentration of about 10% of the ideal one. The threshold concentration for initiating the FM coupling will be $4 \times 10^{19} \times 0.10 = 4 \times 10^{18}$.

By further increasing oxygen defects, the VRH spheres strongly overlap with one another and the BMP spheres start to contact one another, the strongest conduction-FM state can be expected, shown as the third case in Table I, and the “conduction FM” state in Fig. 4. In this case, the distance between defects is much closer at 1.52 nm and with a carrier concentration as high as $1.4 \times 10^{20} \text{ cm}^{-3}$, and the sample can be considered as a conducting quasimetal. At this point, the VRH model may not be a suitable description. If, however, the defect concentration keeps increasing and if the crystal structure remains intact, a very strong Coulomb coupling between localized carriers may initiate a direct interaction between the spins of adjacent localized carriers. This direct coupling can result in an antiparallel configuration of BMP spheres, shown as the “AFM” state in Fig. 4, that reduces the magnitude of the magnetization of the film to a minimum

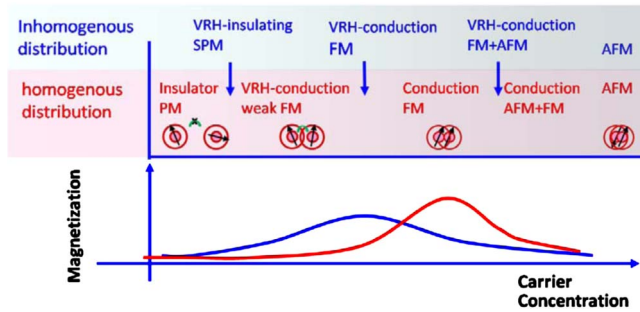


FIG. 4. (Color online) Evolution of the electric and magnetic phases and the magnetization of the DMS film as a function of the carrier concentration in a uniform (red) and an inhomogeneous (blue) distribution.

value. Of course, in the presence of an inhomogeneous distribution of defects, the antiparallel clusters may occur at a lower carrier concentration.

The major issue in DMS is the ratio of the spin current, which is one of the major mechanisms that applications depend on. In most cases, the radius of BMP is smaller than the radius of the outer sphere in the present concentric bounded model. Any hopping not directly between two BMP spheres will lose its spin coherence unless the material has a high polarization, such as EuO .³³ The spin-current ratio is, therefore, strongly associated with the ratio of the inner and outer radii. On the other hand, one may reduce the radius of the outer concentric sphere, by increasing the density of state at the Fermi energy, to meet that of the BMP sphere to increase the spin-coherent hopping and the ratio of spin current.

IV. CONCLUSIONS

In this study, an electric field effect is applied to Co:ZnO films as an example to demonstrate the model we presented.

The carrier concentration of the film with fixed oxygen vacancies and magnetic dopants can be injected in or extracted from the films by the electric field effect. With the change in carrier concentration, the saturated magnetization and coercivity remain unchanged, while the magnetization curves saturate faster for carrier extraction or slower for carrier injection. These magnetic phenomena can be fully explained by the BMP model with the change in radius of the localized carriers due to the external change in carrier concentration. However, the availability of Mott's variable-range hopping in fitting the resistivity to temperature curves indicates that the localized radii of the localized carriers are larger than that of the BMP model. Based on these experiment results, a concentric bounded model is proposed in this study. In this model, carriers are localized around a defect, in which the localized carrier strongly couples to the doped magnetic iron, forming a bounded magnetic polaron in the inner sphere and can only itinerate with no spin coherence in the outer shell. Carriers can move either by the spin-polarized or spin-independent variable-range hopping between concentric spheres. With this model, we are able to qualitatively understand both the magnetic and electric conduction properties of oxide DMS and to introduce the evolution of both properties as a function of the defect concentration. The spin-current ratio can be enhanced by increasing the spin splitting or the density of state at the Fermi level. To quantitatively understand the mechanism of oxide DMS, the conduction of carriers must be included in more detailed models, such as those being developed by Calderon and Das Sarma³⁴ and Yu *et al.*¹¹

ACKNOWLEDGMENTS

Great appreciation is due to S. J. Sun for sharing his theoretical opinions of this paper. This project is supported by the National Science Council of Taiwan under Grant No. NSC-95-2112-M-110-011-MY3.

*Corresponding author; hchou@mail.nsysu.edu.tw

¹J. K. Furdyna, *J. Appl. Phys.* **64**, R29 (1988).

²H. Munekata, H. Ohno, S. von Molnar, A. Segmüller, L. L. Chang, and L. Esaki, *Phys. Rev. Lett.* **63**, 1849 (1989).

³H. Ohno, H. Munekata, T. Penney, S. von Molnar, and L. L. Chang, *Phys. Rev. Lett.* **68**, 2664 (1992).

⁴H. Ohno, A. Shen, F. Matsukura, A. Oiwa, A. Endo, S. Katsumoto, and Y. Iye, *Appl. Phys. Lett.* **69**, 363 (1996).

⁵S. A. Wolf, D. D. Awschalom, R. A. Buhrman, J. M. Daughton, S. von Molnar, M. L. Roukes, A. Y. Chtchelkanova, and D. A. Treger, *Science* **294**, 1488 (2001).

⁶T. Dietl, H. Ohno, F. Matsukura, J. Cibert, and D. Ferrand, *Science* **287**, 1019 (2000).

⁷T. Dietl, *Nat. Mater.* **2**, 646 (2003).

⁸Kevin R. Kittilstved, William K. Liu, and Daniel R. Gamelin, *Nat. Mater.* **5**, 291 (2006), and references cited therein.

⁹J. R. Neal, A. J. Behan, R. M. Ibrahim, H. J. Blythe, M. Ziese, A. M. Fox, and G. A. Gehring, *Phys. Rev. Lett.* **96**, 197208 (2006), and references cited therein.

¹⁰N. Khare, M. J. Kappers, M. Wei, M. G. Blamire, and J. L. MacManus-Driscoll, *Adv. Mater. (Weinheim, Ger.)* **18**, 1449 (2006), and references cited therein.

¹¹C. F. Yu, T. J. Lin, S. J. Sun, and H. Chou, *J. Phys. D* **40**, 6497 (2007).

¹²D. J. Priour, Jr., E. H. Hwang, and S. Das Sarma, *Phys. Rev. Lett.* **92**, 117201 (2004).

¹³Kevin R. Kittilstved, Dana A. Schwartz, Allan C. Tuan, Steve M. Heald, Scott A. Chambers, and Daniel R. Gamelin, *Phys. Rev. Lett.* **97**, 037203 (2006).

¹⁴K. A. Griffin, A. B. Pakhomov, C. M. Wang, S. M. Heald, and Kannan M. Krishnan, *Phys. Rev. Lett.* **94**, 157204 (2005).

¹⁵K. Sato and H. Katayama-Yoshida, *Semicond. Sci. Technol.* **17**, 367 (2002).

¹⁶S. A. Chambers, D. A. Schwartz, W. K. Liu, K. R. Kittilstved, and D. R. Gamelin, *Appl. Phys. A: Mater. Sci. Process.* **88**, 1 (2007).

¹⁷A. Chattopadhyay, S. Das Sarma, and A. J. Millis, *Phys. Rev. Lett.* **87**, 227202 (2001).

- ¹⁸M. J. Calderon, G. Gomez-Santos, and L. Brey, *Phys. Rev. B* **66**, 075218 (2002).
- ¹⁹A. Kaminski and S. Das Sarma, *Phys. Rev. Lett.* **88**, 247202 (2002).
- ²⁰T. Dietl and J. Spalek, *Phys. Rev. Lett.* **48**, 355 (1982).
- ²¹P. Mahadevan, A. Zunger, and D. D. Sarma, *Phys. Rev. Lett.* **93**, 177201 (2004).
- ²²C. H. Park and D. J. Chadi, *Phys. Rev. Lett.* **94**, 127204 (2005).
- ²³M. Venkatesan, C. B. Fitzgerald, J. G. Lunney, and J. M. D. Coey, *Phys. Rev. Lett.* **93**, 177206 (2004).
- ²⁴J. M. D. Coey, M. Venkatesan, and C. B. Fitzgerald, *Nat. Mater.* **4**, 173 (2005).
- ²⁵A. C. Durst, R. N. Bhatt, and P. A. Wolff, *Phys. Rev. B* **65**, 235205 (2002).
- ²⁶H. Toyosaki, T. Fukumura, Y. Yamada, K. Nakajima, T. Chikyow, T. Hasegawa, H. Koinuma, and M. Kawasaki, *Nat. Mater.* **3**, 221 (2004).
- ²⁷J. C. A. Huang, H. S. Hsu, Y. M. Hu, C. H. Lee, Y. H. Huang, and M. Z. Lin, *Appl. Phys. Lett.* **85**, 3815 (2004).
- ²⁸H. S. Hsu, J. C. A. Huang, Y. H. Huang, Y. F. Liao, M. Z. Lin, C. H. Lee, J. F. Lee, S. F. Chen, L. Y. Lai, and C. P. Liu, *Appl. Phys. Lett.* **88**, 242507 (2006).
- ²⁹R. Ramesh and Nicola A. Spaldin, *Nat. Mater.* **6**, 21 (2007); D. C. Look, J. W. Hemsky, and J. R. Sizelove, *Phys. Rev. Lett.* **82**, 2552 (1999).
- ³⁰N. F. Mott and E. A. Davies, *Electronic Processes in Noncrystalline Solids*, 2nd ed. (Oxford University, New York, 1979).
- ³¹M. Viret, L. Ranno, and J. M. D. Coey, *Phys. Rev. B* **55**, 8067 (1997).
- ³²Shinji Kuroda, Nozomi Nishizawa, Kôki Takita, Masanori Mitome, Yoshio Bando, Krzysztof Osuch, and Tomasz Dietl, *Nat. Mater.* **6**, 440 (2007).
- ³³A. Schmehl, V. Vaithyanathan, A. Herrnberger, S. Thiel, C. Richter, M. Liberati, T. Heeg, M. Ruckerath, L. F. Kourkoutis, S. Muhlbauer, P. Boni, D. A. Muller, Y. Barash, J. Schubert, Y. Idzerda, J. Mannhart, and D. G. Schlom, *Nat. Mater.* **6**, 882 (2007).
- ³⁴M. J. Calderon and S. Das Sarma, *Ann. Phys.* **322**, 2618 (2007).